Hydraulic conductivity and microstructure changes of compacted bentonite/sand mixture during hydration

Qiong Wang, Yu-Jun Cui, Anh Minh A.M. Tang, Jean-Dominique Barnichon, Simona Saba, Wei-Min Ye

Hydraulic conductivity and microstructure changes of compacted bentonite/sand mixture during hydration

Qiong Wang[1], Yu-Jun Cui[1,3], Anh Minh Tang[1], Jean-Dominique Barnichon [2], Simona Saba[1] Wei-Min Ye[3]

[1] *Ecole des Ponts ParisTech, Laboratoire Navier/CERMES, France*

[2] *Institut de Radioprotection et Sureté Nucléaire (IRSN), France*

[3] *Tongji University, China*

Corresponding author:
Prof. Yu-Jun CUI
Ecole des Ponts ParisTech
6-8 av. Blaise Pascal, Cité Descartes, Champs-sur-Marne
77455 Marne-La-Vallée
France

Telephone : +33 1 64 15 35 50
Fax : +33 1 64 15 35 62
E-mail : yujun.cui@enpc.fr

Abstract:

Compacted bentonite-based materials are often considered as sealing/backfill materials in deep geological repository for high level radioactive waste. A good understanding of their hydration process is essential as this process is directly related to over-pack corrosion and nuclide migration. In this study, the unsaturated hydraulic properties of MX80 bentonite/sand mixture were characterized by carrying out a series of experiments including water retention test, infiltration test as well as microstructure observation. It was found that with suction decrease under constant volume condition, the hydraulic conductivity decreased followed by an increase after a suction threshold. At suctions higher than 12.6 MPa, hydration led to progressive large-pores clogging by exfoliation of clay particles. On the contrary, when saturation was approached (suction lower than 4.2 MPa), the large-pores quantity increased due to the creation of two-dimensional pores. It was also observed that the soil hydraulic conductivity changed following the same tendency as the large-pores quantity during hydration. In other words, water transfer was primarily governed by the network of large-pores.

Keywords: bentonite/sand mixture; suction; constant-volume condition; hydraulic conductivity; microstructure

1 INTRODUCTION

Most concepts of deep geological repository for high level radioactive waste are based on the multi-barrier system consisting of the natural barrier (host rock) and engineered barriers (waste container, buffer and sealing elements). One of the most important functions of the engineered barrier is to create a zone of low permeability for separating the high-level radioactive waste from the surrounding environment (Komine, 2010). Bentonite-based materials are often chosen as sealing/backfill materials in this multi-barrier system due to their low permeability, high swelling and high radionuclide retardation capacities (Pusch, 1979; Yong et al., 1986; Villar et al., 2008).

Once emplaced in the repository, the bentonite-based materials start to be hydrated by the pore water infiltrating from the host-rock. These materials absorb water and swell. Firstly, the technological voids are filled up, with a decrease in dry density. Then, the subsequent swelling is restrained by the host rock and swelling pressure develops under constant volume conditions. The hydration under this constant volume condition corresponds to a coupled hydro-mechanical process with involvement of microstructure changes. A proper understanding of this process is essential for well controlling the water transfer-related phenomena as over-pack corrosion, nuclide migration, etc.

A number of studies have been performed to study the water transfer in bentonite-based materials in both saturated state (Kenney et al., 1992; Dixon et al.,

1999; Komine, 2004, etc) and unsaturated state (Börgesson, 2001; Loiseau et al., 2002; Kröhn, 2003a, 2003b; Lemaire et al., 2004; Cui et al., 2008). The saturated hydraulic conductivity has been found to be strongly dependent on the initial dry density (Dixon, 1999; Karnland et al., 2008, etc.). Under unsaturated conditions with suction-dependent water flow, the hydraulic conductivity was often determined using the instantaneous profile method (Daniel, 1982). Following this method, Cui et al. (2008) investigated the unsaturated hydraulic conductivity of the Kunigel bentonite/sand mixture and observed that with suction decrease under constant volume conditions, the hydraulic conductivity decreases followed by an increase after certain suction threshold. Ye et al. (2009) obtained similar results on GMZ bentonite. Thomas et al. (2003) and Villar et al. (2005) also pointed out that, in expansive materials, hydraulic conductivity decreases with the increase in degree of saturation, due to microstructural modifications. This is different from the common results showing that the hydraulic conductivity of unsaturated soils increases with suction decrease (van Genuchten, 1980; Fredlund and Rahardjo, 1993). The particular trend observed for bentonite-based materials adds a degree of complexity when dealing with the long term behaviour of these materials. Without considering this phenomenon, the water transfer in bentonite-based materials will be over-estimated. Thus, it is of great importance to go in depth of this phenomenon by considering the coupled hydro-mechanic changes during the hydration process.

If the phenomenon of the particular hydraulic conductivity changes with suction decrease for bentonite-based materials was evidenced experimentally (Cui et al., 2008;

93 Ye et al.; 2009), the explanation has been not yet confirmed by microstructure
94 analysis. The present study aims at completing this lack by investigating the hydraulic
95 properties of a compacted bentonite-sand mixture and the microstructure changes
96 during the hydration process. Infiltration test and water retention test were first carried
97 out under constant volume conditions allowing the determination of hydraulic
98 conductivity by the instantaneous profile method. The study was then completed with
99 the microstructure observation allowing analysing the effect of microstructure change
100 on the variations of hydraulic conductivity. All tests were carried out at constant
101 ambient temperature (20±1°C), and the effect of temperature was not considered in
102 this study.

103 # 2 MATERIALS AND METHODS

104 ## 2.1 Materials and samples preparation

105 The soil studied is a mixture of MX80 bentonite and quartz sand with a proportion of
106 70/30 in dry mass. The bentonite is from Wyoming, USA, with a high content of
107 montmorillonite (80%). It has a liquid limit of 575%, a plastic limit of 53% and a unit
108 mass of 2.77 Mg/m^3. The cation exchange capacity (CEC) is 76 meq/100g (83 % of
109 Na^+). The grain size distribution (Figure 1) determined by hydrometer (French
110 standard AFNOR NF P94-057) on deflocculated clay shows that the fraction of
111 clay-size particles (< 2 μm) is 84%.

112 The sand used in the mixture was from Eure and Loire (France), with a unit mass of
113 sand grains of 2.65 Mg/m^3. It was sieved at 2 mm prior to being mixed with the

bentonite. Figure 1 shows the grains size distribution curve determined by the dry sieving method (AFNOR NF P94-056). The curve for sand is characterized by a uniformity coefficient C_u of 1.60 and a D_{50} close to 0.6 mm. This curve is close to that of bentonite powder obtained by "dry" sieving (see in Figure 1).

Synthetic water having similar chemical composition to that of the pore water of the Callovo-Oxfordian claystone (TDS = 5.7 g/L) from the ANDRA Underground Research Laboratory (URL) in Bure (France) was used for the infiltration test (Table 1). For the preparation of the synthetic water, the chemical components in powder were mixed with distilled water using a magnetic stirrer until full dissolution.

For the samples preparation, the bentontie powder has a hydroscopic water content of 12.2% was carefully mixed with dry sand (70% bentonite - 30% sand in mass) giving a mixture at a water content of 8.5%. The mixture powder was then put into a hermetic container connected to a vapor circulation system containing free water (100% relative humidity), so as to reach a target water content of 11.0%. The grain size distribution curve of the mixture powder is presented in Figure 1. It shows a well graded distribution around a mean diameter of 0.9 mm.

The soil specimens for both the infiltration and water retention tests were obtained by compaction of the bentonite/sand mixture powder at its water content of 11.0%. A given quantity of the mixture was placed in a metallic mould and statically compacted to a dry density of 1.67 Mg/m^3. The initial suction of the compacted samples was about 65 MPa (measured using a relative humidity sensor after compaction). For the infiltration test, the specimen (250-mm long and 50 mm in diameter) was compacted

136 in 5 layers of 50-mm thickness each.

137 **2.2 Experimental method**

138 The hydraulic conductivity of the unsaturated bentonite/sand mixture was determined
139 using the instantaneous profile method, which requires both suction and volumetric
140 water content profiles (Daniel, 1982; Cui et al., 2008; Ye et al., 2009). The suction
141 profile (corresponding to the total suction) was obtained by monitoring the relative
142 humidity (RH) changes in an infiltration test, whereas the volumetric water content
143 profile was deduced from the water retention curve determined separately.

144 **2.2.1 Infiltration test**

145 The hydration cell used for the infiltration test is presented in Figure 2. After
146 compaction, the soil specimen (50 mm in diameter and 250-mm long) was carefully
147 introduced into the cylindrical cell (50 mm in inner diameter) with the ends of the two
148 cells jointed together. The hydration cell is made of stainless steel, which hindered
149 any lateral volume changes. Four relative humidity (RH) sensors were installed every
150 50 mm along the sample (h = 50, 100, 150, 200 mm from the wetting end) through the
151 ports in the wall of the cell. The RH sensor consists of a unique capacitive sensor
152 element for RH measurement and a stainless steel shell (12 mm in external diameter)
153 for protecting the sensors from deformation and corrosions. Two ends of the cell were
154 tightly closed by metallic discs of 40 mm thickness each. Water supply was done at
155 the atmospheric pressure through the water inlets in the bottom base, which was
156 connected to burettes. The top cover has an outlet for air expulsion. To avoid water

157 evaporation, a deflated balloon-shaped membrane was used to cover the air outlet.
158 The air in the membrane was released regularly in order to keep an air pressure close
159 to the atmospheric one. The water volume injected into the sample was also measured
160 during the test by monitoring the water level in the burettes.

161 At the end of the infiltration test, the sample was extruded by pushing the top side,
162 about 12 MPa pressure was applied for this purpose. Several small specimens at
163 different positions along the column were taken for the water content and dry density
164 determinations. The water content of the sample was measured by oven drying, while
165 the dry density was determined based on the fluid displacement technique (see Head,
166 1980, Geiser, 1999) using an immiscible oil Kerdane (with a density of 0.791 at
167 20^{o}C).

168 **2.2.2 Water retention curve**

169 The water retention curve of the bentonite/sand mixture under constant volume
170 condition was determined by controlling the suction using both the vapour
171 equilibrium technique (for suctions higher than 4.2 MPa) and osmotic technique (for
172 suctions of 1 and 0.1 MPa). It is worth noting that the vapour equilibrium technique
173 controls total suction whereas the osmotic technique controls matric suction (see
174 Delage 1998a; Delage and Cui, 2008; Blatz et al.; 2008 for more detailed). The zero
175 suction was imposed by injecting the synthetic water (Table 1) into the sample.

176 The compacted sample (50 mm in diameter and 5 mm in height) was placed in a
177 stainless steel cell. Two porous disks were put at both sides of the sample allowing

178 vapour or water flow. To apply the osmotic technique, a semi-permeable membrane
179 was placed between the porous stone and the soil sample (Figure 3a), the whole was
180 then sandwiched between two perforated discs and immerged in a PEG 20 000
181 (Polyethylene Glycol) solution at a concentration corresponding to the required
182 suction (see Table 2). Several drops of penicillin were added in the solution to prevent
183 from attack of bacteria. To apply suction with the vapour equilibrium technique, the
184 sample sandwiched between two porous stones was installed between two external
185 plates with valves (Figure 3b) that were connected to a device containing a saturated
186 salt solution for relative humidity control (see Wang et al., 2012 for more details).
187 Following this technique, 2-4 weeks was required to reach the equilibrium (Marcial,
188 2003; Tang & Cui, 2005). However, the equilibrium time was much shorter for the
189 osmotic technique as it allows liquid water exchanges between the soil sample and the
190 PEG solution (Blatz et al., 2008). In this study, the equilibration time was extended to
191 2 months for both the vapour equilibrium technique and osmotic technique and the
192 water content of all samples was determined by weighing at the end.

193 All water retention tests performed and the solutions used for suction control are
194 presented in Table 2. As shrinkage may occur upon drying, it was not possible to
195 control sample volumes along drying paths. Thus, only the wetting curve was
196 determined under restrained-swell conditions. This was enough for the purpose of
197 hydraulic conductivity determination based on the infiltration test under constant
198 volume conditions.

2.2.3 Microstructure observation

Mercury Intrusion Porosity (MIP) and Scanning Electron Microscope (SEM) tests were carried out on freeze-dried samples, which had been equilibrated at different suctions under constant volume conditions. The suction values considered ranged from 65 MPa (as-compacted state) to zero (saturated state). For as-compacted samples, it was cut to small slices and freeze-dried (see Delage & Lefevbre, 1984; Cui et al., 2002., Delage et al., 2006; Tang et al., 2011 for more details). Samples for other suctions were taken from the water retention test under constant volume conditions (Table 2 for details). Each sample was cut to two parts, one for the preparation of samples for the microstructure observation and another for water content determination by weighing (for water retention curve).

3 EXPERIMENTAL RESULTS

Figure 4 depicts the water retention curve (suction versus the gravimetric water content) obtained along the wetting path under constant-volume conditions. In the plane of gravimetric water content versus suction (Figure 4), a bi-linear water retention curve was obtained: water content increases linearly with suction decrease when this latter is higher than 1 MPa; at lower suctions the water content remains constant and the water retention curve is almost horizontal. The inflexion of the WRC (1 MPa) can be considered as the air-entry value of the sample.

At the end of the infiltration test, the sample was removed by pushing it from the top.

219 The water content and dry density along the column were determined and shown in
220 Figure 5. As expected, the water content decreased with increasing distance from the
221 wetting end. Regarding the dry density distribution, a lower dry density than at the
222 initial state (1.62-1.65 Mg/m^3 against 1.67 Mg/m^3) was obtained in the near wetting
223 end zone (h = 0-40 mm); a dry density close to the initial one (1.67-1.68 Mg/m^3
224 against 1.67 Mg/m^3) was obtained in the middle zone (h = 50-150 mm); in the upper
225 zone (h = 200 - 250 mm), a significant dry density increase up to 1.73 Mg/m^3 was
226 identified.

227 During the infiltration test, RH changes over time were monitored and plotted in
228 Figure 6 for all measurement positions (h = 50, 100, 150 and 200 mm). The initial RH
229 was 62 ± 1% corresponding to a suction of 64.5 ± 1.5 MPa. Once the infiltration
230 started, the value of the RH at h = 50 mm increased rapidly and reached 90% after
231 500 h, then increased gradually to 98.30% after 1900 h. The value of the sensors at h
232 = 100, 150 and 200 mm started to increase after about 200 h, 500 h and 1900 h
233 respectively. The larger the distance from the wetting end the lower the increasing rate
234 of RH.

235 The total suction (s) was then calculated from RH value using Kelvin's law:

236 $$s = -(\rho_w RT / M_w)\ln(RH/100) \quad \text{Eq. (1)}$$

237 where ρ_w is the water unit mass (1 Mg/m^3); R is the universal (molar) gas constant
238 (8.31432 J/mol K); T is the absolute temperature (K), equal to (273.15+20) ^{o}C in this
239 study; M_w is the molecular mass of water vapour (18.016 kg/kmol).

Figure 7 depicts the suction isochrones for every 400 h. Note that the suction value at h = 250 mm was not monitored and it was estimated by linearly extending the curves between h = 150 mm and h = 200 mm. At t = 0, the initial suction of the sample was quite homogeneous, with a mean value of 64.5 ± 1.5 MPa. It was supposed that after starting the infiltration, the suction at the wetting face h = 0 mm decreased rapidly to zero. The total suction at h = 50 mm decreased to 2.37 MPa at t = 2200 h while the total suction at h = 200 mm started to decrease at t = 1900 h, and remained high (s = 33.84 MPa) at t = 6000 h.

Based on the suction profiles (Figure 7), the hydraulic gradients (i) and water fluxes (q) at each measurement section (h) and time (t) were deduced following the methods shown in Figure 8. The hydraulic gradients were calculated as the tangent of suction profiles (s and h are expressed in m) as indicated in Figure 8a and the water fluxes were determined by integrating the difference in the volumetric water content profiles at a time interval (Δt) as indicated in Figure 8b.

To calculate the water flux, the volumetric water content of the mixture was deduced from the total suction using the water retention curve obtained at constant-volume conditions (Figure 4). As the suction measured by RH sensors in the infiltration test ranges from 2.37 MPa to 65 MPa, Eq. 2 (see also Figure 4) was used to calculate the gravimetric water content from suction, and the volumetric water content (θ) can be then calculated using Eq.3:

$$w = -7.261 Log(\mathrm{s}) + 24.102 \quad \text{(Eq. 2)}$$

$$\theta = w\rho_d / \rho_w \quad \text{(Eq. 3)}$$

where, ρ_d is assumed to be constant (1.67 Mg/m^3) during infiltration under constant volume conditions.

In order to verify the validity of these calculations, the total volume of water passing through each section was calculated from the volumetric water content profiles. The sum of these volumes from h = 0 mm to h = 250 mm corresponds to the volume of water absorbed by the soil specimen during infiltration. Figure 9 shows the comparison between the injected volume of water and that estimated from the water content profiles. It can be observed that there is a good agreement between the measured and calculated values, confirming the validity of the analyses performed.

Using the suction profiles presented in Figure 7, the hydraulic gradient (i) and water fluxes (q) at the four measurement sections h = 50 mm, 100 mm, 150 mm and 200 mm for each 100 h were obtained, and used to calculate the hydraulic conductivity by applying Darcy's law (Eq.4). The hydraulic conductivity determined is plotted versus suction in Figure 10. It can be seen that at different measurement sections different relationships were obtained.

$$k_w = -\frac{1}{A} \cdot \frac{q}{\frac{1}{2}(i_t + i_{t+\Delta t})} \qquad \text{(Eq. 4)}$$

where, k_w is the hydraulic conductivity; i_t and $i_{t+\Delta t}$ are the hydraulic gradients at instant t and $t+\Delta t$, respectively.

The pore size distribution curves for suctions ranging from 65 MPa (initial state) to 12.6 MPa are presented in Figure 11a and Figure 11b. It was observed in Figure 11a

282 that the final values of the intruded mercury void ratio (e_{mi}) were lower than the
283 global soil void ratio (e = 0.63). Moreover, the amount of non-intruded porosity (e_{mi} =
284 0.47 in the initial state) decreased with suction decrease. From the derivative curves
285 (Figure 11b), a typical bimodal porosity was identified in the initial state (ρ_d = 1.67
286 Mg/m^3, s = 65 MPa), and two pore groups can be defined: small-pores having a mean
287 size of 0.02 µm and large-pores having a mean size of 50 µm. Following the
288 classification detailed in Stepkowska (1990) and Villar et al. (2012), these two pore
289 families correspond to the categories of mesopores (0.002-0.05 µm) and macropores
290 (> 0.05 µm), respectively. The application of 38 MPa suction resulted in significant
291 decrease of large-pores quantity (about 10%), and little changes in small-pores
292 (Figure 11b). However, no obvious further changes in both the large-pores and
293 small-pores can be observed for the subsequent decrease of suction (38 - 24.8 - 12.6
294 MPa).

295 Figures 11c and 11d show the curve for 4.2, 1 and 0 MPa suction, lower values of
296 non-intruded void ratio e_{mi} were also obtained compared to the global void ratio of the
297 soil (Figure 11c). However, it was found that the intruded porosity at these suctions
298 was slightly higher than that in the initial state (s = 65 MPa, e_{mi} = 0.47). From the
299 derivative curves (Figure 11d), it was clearly seen that this increased intruded porosity
300 corresponded to the difference in large-pores volume, as the small-pores volume
301 decreased with decreasing suction. Moreover, a third pore family (with pore size of
302 0.1-2 µm) appeared for the saturated sample.

303 The pore size distribution analyse was completed using the SEM technique (Figure
304 12). The photos were taken at two scales which focused on the behaviour of mixture
305 (1250 x 1000 µm) and bentonite aggregates (25 x 20 µm), respectively. The sand
306 grains cannot be identified in the photos at lower magnification (picture size of 1250 x
307 1000 µm). The photograph taken at the initial state (s = 65 MPa) clearly shows the
308 large-pores with a maximum diameter of about 100 µm (Figure 12a), which is in
309 agreement with the MIP results from Figure 11a. Figure 12b shows that the
310 aggregates were densely assembled. The small-pores observed in the MIP test (0.02
311 µm) cannot be detected by the SEM technique. Comparison of the photographs of 38
312 MPa suction (Figure 12d) and 65 MPa suction (Figure 12b) shows that the clay
313 particles exfoliation occurred when suction decreased. The photographs at saturated
314 state (Figure 12e and 12f) show that the large-pores observed at higher suctions
315 (Figure 12a and 12c) were filled by the swollen bentonite; however, there are
316 fissure-like (with very large aspects ratio) 2-dimensional pores (2-D pores) which
317 correspond to the pore group with a mean diameter of 50 µm and 1 µm observed in
318 Figure 11d. Audiguier et al. (2008) observed similar 2-D pores of a diameter between
319 0.1 and 1 µm in a natural clay after free swelling.

320 # 4 INTERPRETATION AND DISCUSSION

321 After the infiltration test, a decrease of dry density was observed in the lower part (h =
322 0-40 mm), a dry density close to the initial was obtained in the middle zone (h =
323 50-150 mm). Several authors (Lemaire et al., 2004; Kröhn, 2003b, 2004; Villar et al.,

2008) reported that swelling leads to a displacement of clay particles in the near wetting end zone, and thus to a significant decrease of dry density. This in turn causes compaction of the bentonite in the still dry parts. This was obviously not the case in this study because the resulting compaction in the middle zone was not noticeable: the value of dry density remained the same after the test. Thereby, the decrease of dry density in the near wetting end zone may probably due to the soil rebounding due to the release of swelling pressure. The limited compaction by soil swelling pressure can be also explained by the fact that the compaction pressure applied for sample preparation was about 12 MPa, much higher that the soil swelling pressure estimated at 3 MPa at 1.67 Mg/m^3 dry density (see Wang et al. 2013). As far as the upper part (200-250 mm) is concerned, the significant increase of dry density is rather related to the sample removal. As described previously, the sample was extruded by pushing the top side with a pressure as high as 12 MPa. This pressure was almost the same as the pressure applied for the sample compaction. If we consider a yield stress of 12 MPa for the sample at its initial state, the value must decrease upon hydration. Therefore, significant compaction can be expected during sample extrusion. However, this compaction was limited to the upper part because of the contribution of the friction between the sample and the metallic column. Kröhn (2003b, 2004) performed a laboratory infiltration test on MX80 bentonite with an initial dry density of 1.50 Mg/m^3 and observed similar phenomenon: significant decrease of dry density occurred in the area near the wetting end (20 mm for a sample of 100 mm long); no-noticeable changes occurred in the remaining part. In addition, all density changes

346 took place within the first four days, with no time dependence (over 189 days).
347 Thereby, they considered that the assumption of no migration of bentonite particles in
348 the specimen is a good approximation except for the first few millimeters (Kröhn,
349 2004). Therefore, in the test conditions adopted in the present work, it is believed that
350 the error was very limited when determining the hydraulic conductivity by taking the
351 mean value of dry density (1.67 Mg/m^3).

352 From the shape of the suction isochrones shown in Figure 7, it can be observed that
353 suction changes mainly occurred in the lower part of the sample below 100 mm, and
354 in the upper part limited changes were identified. This is in agreement with the water
355 content distribution curve (Figure 5a), where much more change near the wetting end
356 was observed. As noted by Delage et al. (1998a, b) and Ye et al. (2009), this
357 phenomenon could be explained by separating the liquid water transfer from the water
358 vapour diffusion: in the zone near the wetting face, the water transfer involves mainly
359 the liquid water; by contrast, water vapour diffusion prevails in the zone far from the
360 wetting face. In fact, infiltration tests performed by Delage et al. (1998a, b) showed
361 almost vertical suction profiles in all time within the part beyond 50 mm from the
362 wetting face. As the suction was deduced from the measured relative humidity, they
363 concluded that at the upper part beyond 50 mm, the water transfer was mainly
364 governed by vapour diffusion. The less vertical suction profiles in the present work
365 suggest a relatively less prevailing vapour transfer than that in the case of Delage et al
366 (1998a, b).

By applying Darcy's law, different relationships between hydraulic conductivity and suction were obtained at different measurement sections (Figure 10). As reported by Loiseau et al. (2002), Cui et al., (2008) on the Kunigel/sand mixture and Marcial (2003) on the pure MX80 bentonite, this phenomenon is related to the effect of hydraulic gradient. In general, when experimentally determining the hydraulic conductivity based on Darcy's law, a linear relationship between water flow rate (q) and hydraulic gradient (i) is obtained. However, non-linear relationships are often observed for clayey soils (Lutz & Kemper, 1959; Miller & Low, 1963; Zou, 1996), and there is a "critical gradient" below which flow occurs in non-Darcian mode (Yong and Warkentin, 1975; Dixon et al., 1987). This can be explained by the high energy of the water adsorbed in clays, which increases with the clay fraction and activity (Dixon et al., 1987). When the hydraulic gradient increases, this energy is overcome locally and the adsorbed water can be mobilised. For soils containing highly active clay minerals such as smectite in this study, this critical gradient effect can be significant leading to different k - s relationships obtained at different measurement sections.

For clarifying this effect, the water fluxes (q) and hydraulic gradient (i) for each suction level (suction from 62 to 32 MPa) are plotted in Figure 13. Bi-linear relationships can be observed for each suction value, indicating existence of "critical gradients", their values ranging from 8000 to 38000. To apply Darcy's law, the water flow was considered only when the linear segment at higher water flux was reached (details about this method can be found in Dixon et al., 1992).

388 Considering the critical gradient effect (Figure 13), the hydraulic conductivity was
389 corrected and shown in Figure 14. A unique relationship was obtained between
390 hydraulic conductivity and suction, independent of the measurement sections. In
391 Figure 14, the hydraulic conductivity determined by Karnland et al. (2008) for the
392 same material at the same dry density (1.67 Mg/m^3) under saturated state is also
393 presented: a much higher value of 10^{-13} m/s was observed. Unlike the non swelling
394 soils for which the hydraulic conductivity is increasing upon wetting, a "U-shape"
395 relationship was observed: the hydraulic conductivity decreased when suction
396 decreased from 65 to about 15 MPa, then increased for further suction decrease.
397 Similar observations were made on the Kunigel-V1/sand mixture (JNC, 2000; Cui et
398 al., 2008) and GMZ bentonite (Ye et al., 2009). As explained by Cui et al. (2008) and
399 Ye et al. (2009), in the beginning water transfer was primarily governed by the
400 network of large-pores, which were progressively clogged by the expanding hydrated
401 aggregates, leading to the hydraulic conductivity decrease. When the large-pores
402 clogging ended and water transfer was controlled by the suction gradient, the common
403 hydraulic conductivity increase with suction decrease was observed.

404 It was observed in Figure 11a that the intruded mercury void ratio (e_{mi}) were lower
405 than the global soil void ratio (e = 0.63). This can be explained by the limited pressure
406 range of the MIP technique: for the high-plasticity soils, there is a significant pore
407 volume (entrance diameter smaller than 6 nm) that the mercury could not penetrate to
408 (Lloret et al., 2003; Delage et al., 2006). Comparison of the curves at different
409 suctions shows that with decreasing suction (65-38-24.9-12.6 MPa), the amount of

intruded porosity decreases. Pusch (1999) and Cui et al. (2002) observed the same phenomenon and explained by the interaction between large- and small-pores: during suction decrease under constant-volume conditions the size of non-intruded pores increased with increasing interlayer space, while the large-pores were filled by small clay particles.

Figure 11b showed that suction decrease did not change the small-pores family, whereas a decrease of large-pores quantity was observed - it was significant when suction decreased from 65 MPa to 38 MPa (10%) and much less (3%) for the subsequent suction decrease (38-24.8-12.6 MPa). This confirms the previous conclusion that during suction decrease the large-pores were clogged (although at different rate) by the invasion of exfoliated clay particles whose interlaminar distance increases upon saturation. This phenomenon could also be identified in the SEM photograph with high magnification for 38 MPa suction (Figure 12d).

For suction lower than 4.2 MPa (Figure 11c), a lower value of e_{mi} was also obtained compared to the global void ratio (e = 0.63). However, the intruded porosity at these suctions (4.2, 1 and 0 MPa) was slightly higher than that in the initial state (s = 65 MPa, e_{mi} = 0.47). This phenomenon can be attributed to the larger pore quantity of the pore group having a mean size of 50 µm (for 4.2 and 1 MPa suction) and 1 µm (for zero suction) compared with the initial state (Figure 11d). These two pores groups were identified as 2-D pores of about 50 and 1 µm diameter for the saturated sample in Figure 12e and 12f, respectively. Audiguier et al. (2008) explained the formation of

431 the 2-D pores by the division of clay particles within the aggregates due to swelling.
432 Moreover, the small deformation induced by the release of swelling pressure before
433 freeze-drying may also play a role in the large-pores quantity increase. However, this
434 slight effect could not be identified by the current technique of samples preparation,
435 and new methods without stress state changes are needed to obtain more accurate
436 microstructure observations.

437 It appeared that the small-pores changed only when the saturation was approached (1
438 MPa and 0 MPa in Figure 11 and Figure 12). This phenomenon is in agreement with
439 the conclusion by Cui et al. (2002) for the Kunigel clay/sand mixture: when water
440 infiltrated into the soil, the hydration of clay aggregates hydration started first on the
441 surface giving rise to the clay particles exfoliation and resulting in the clogging of
442 large-pores, whereas the small-pores remained almost un-affected; the small-pores
443 started to change only when the water saturation was approached (suction lower than
444 9 MPa). When saturation was reached, the clay aggregates disappeared (Figure 12f)
445 and a new pore family of about 1 μm diameter was formed, visible from both MIP and
446 SEM tests. The small-pores seemed to be compressed by the swelling pressure,
447 whereas 2-D pores of 1 μm in diameter appeared due to the division of clay particles
448 within the aggregates (Saiyouri et al., 2000).

449 In order to quantify the suction effect on the large-pores, a large-pores radius larger
450 than 2 μm was considered based on the curves in Figure 11where it can be observed
451 that the proportion of pores larger than 2 μm changed with decreasing suction. Using

this limit value that separates large-pores from small-pores, the void ratio corresponding to the large-pores was derived from the cumulative curves (Figure 11). The relationship between the calculated large-pore void ratio (e_L) and applied suction are presented in Figure 15. It can be seen that the large-pores quantity was progressively reduced with decreasing suction in the range of 65 to 12.6 MPa (zone I). However, the subsequently decrease of suction to 4.2 MPa led to an increase of large-pores quantity. This can be explained by the creation of the 2-D pores described above; a significant decrease followed when suction decreased from 1 MPa to zero (zone II).

It is interesting to note that if we relate the large-pore changes (Figure 15) to the hydraulic conductivity changes (Figure 14), it seems that the hydraulic conductivity changed following the same trend as the large-pores quantity during hydration. In other words, water transfer was primarily governed by the network of large-pores in the full suction range, but not controlled by the suction gradient in the lower suction range as mentioned above. The large-pores decreased progressively in quantity due to the clay particles exfoliation occurred on the aggregates surface in the suction range from 65 to 12.6 MPa, leading to a decrease of hydraulic conductivity. When saturation was approached (4.2 - 1 MPa), water transfers through the 2-D pores appeared, leading to an increase in hydraulic conductivity; in saturated state the value can reach as high as 10^{-13} m/s as reported by Karnland et al. (2008). It should be noted that after saturation, the hydraulic conductivity has been found to be time dependent (Loiseau et al., 2002; Cui et al., 2008). It decreased with time due to the re-organization of

474 microstructure over time in the soil sample. After saturation, water in the
475 inter-aggregate pores is not necessarily in equilibrium with the water inside the
476 aggregates in terms of water potential. Thus the water re-distribution occurred inside
477 the soil, leading to a uniform microstructure in long term (Stroes-Gascoyne et al.,
478 2010).

479 # 5 CONCLUSION

480 The hydraulic properties of a compacted bentonite-sand mixture were investigated in
481 the laboratory by carrying out water retention test and infiltration test as well as the
482 microstructure observation. The results obtained allowed relating the variation of
483 hydraulic conductivity to the microstructure changes.

484 During suction decrease (suction higher than 12.6 MPa) the large-pores were clogged
485 progressively by the exfoliated clay particles (although at different rates); however,
486 when saturation was approached (suction lower than 4.2 MPa) large-pores quantity
487 increased again due to the appearance of 2-D pores. The small-pores changed only
488 when saturation was approached.

489 With suction decrease under constant volume condition, the hydraulic conductivity
490 decreased followed by an increase after certain suction threshold. This change
491 followed the same tendency as the large-pores quantity. In other words, water transfer
492 was primarily governed by the network of large-pores. Over time, the hydraulic
493 conductivity is expected to decrease due to the water re-distribution among different

pore families that leads to a uniform microstructure in long term.

ACKNOWLEDGEMENTS

The work was conducted in the framework of the SEALEX project of IRSN and the PHC Cai Yuanpei project (24077QE). The support of the National Nature Science Foundation of China (41030748) and that of the China Scholarship Council (CSC) are also greatly acknowledged.

REFERENCES

AFNOR, 1992. AFNOR NF P94-057, Soils: investingation and testing. Granulometric analysis. Hydrometer method. Association Francaise de Normalisation. France.

AFNOR, 1996. AFNOR NF P94-056, Soils: investigation and testing. Granulometric analysis. Dry sieving method after washing. Association Francaise de Normalisation. France.

Audiguier, M., Geremew, Z., Cojean, R., 2008. Relations enter les microstructures de deux sols argileux de la région parisienne et leur sensibilité au retrait gonflement. SEC2008, Paris, France, 1-3 sept. Editions du LCPC.2008: 235-243.

Blatz, J.A., Cui, Y. J., Oldecop. L., 2008. Vapour Equilibrium and Osmotic Technique for Suction Control. Geotech Geol Eng (2008) 26:661–673.

Börgesson, L., Chijimatsu, M., Fujita, T., Nguyen, T.S., Rutqvist, J., Jing, L., 2001. Thermo-hydro-mechanical characterisation of bentonite-base buffer material by laboratory tests and numerical back analyses. International Journal of Rock Mechanics & Mining Sciences 38, 95-104.

Cui, Y. J., Loiseau, C., Delage, P., 2002. Microstructure changes of a confined swelling soil due to suction controlled hydration Unsaturated soils: proceedings of the Third International Conference on Unsaturated Soils, UNSAT 2002, 10-13 March 2002, Recife, Brazil, 593.

Cui, Y.J., Tang, A..M., Loiseau, C., Delage, P., 2008. Determining the unsaturated hydraulic conductivity of a compacted sand-bentonite mixture under constant-volume and free-swell conditions. Physics and Chemistry of the Earth, Parts A/B/C, 33(Supplement 1):S462 – S471.

Daniel, D.E., 1982. Measurement of hydraulic conductivity of unsaturated soils with thermocouple psychrometers. Soil Science Society of America Journal 20 (6):1125–1129.

Delage, P., Lefebvre, G., 1984. Study of the structure of a sensitive Champlain clay and its evolution during consolidation. Canadian Geotechnical Journal 21 (1), 21–35.

527 Delage P., Howat M., Cui Y.J. 1998a, The relationship between suction and swelling
528 properties in a heavily compacted unsaturated clay. Eng Geol 50(1–2):31–48
529 Delage, P., Cui, Y.J., Yahia-Aissa, M., De Laure, E., 1998b. On the unsaturated hydraulic
530 conductivity of a dense compacted bentonite. Proc. of Unsat'98, Beijing, vol. 1,pp.
531 344–349.
532 Delage, P., Marcial, D., Cui, Y.J., Ruiz, X., 2006. Ageing effects in a compacted bentonite: a
533 microstructure approach. Géotechnique 56 (5), 291–304.
534 Delage P.,Cui Y.J., 2008, An evaluation of the osmotic method of controlling suction,
535 Geomechanics and Geoengineering, 3(1):1-11
536 Dixon, D.A., Cheung, S.C.H., Gray, M.N., Davidson, B.C., 1987. The hydraulic conductivity
537 of dense clay soils. Proc. 40th Canadian Geotechnical Conference, Regina, Saskachewan
538 - Canada, pp. 389–396.
539 Dixon, D.A., Gray, M.N., Hnatiw, D., 1992. Critical gradients and pressures in dense swelling
540 clays. Canadian Geotechnical Journal 29 (6), 1113–1119.
541 Dixon, D.A., Graham, J., Gray, M.N., 1999. Hydraulic conductivity of clays in confined tests
542 under low hydraulic gradients. Canadian Geotechnical Journal 36 (5), 815- 825.
543 Fredlund, D.G., Rahardjo, H., 1993. Soil mechanics for unsaturated soils. John Wiley and
544 Sons, New York
545 GEISER F. 1999, Comportement mécanique d'un limon non saturé:étude expérimentale et
546 modélisation constitutive[D]. Switzerland: Thesis, Ecole Polytechnique Fédérale
547 deLausanne, EPFL.
548 HEAD K H. 1980, Manual of soil laboratory testing, volume 1: soil classification and
549 compaction tests[M]. London: Pentech Press.
550 JNC, 2000. H12: Project to establish the scientific and technical basis for HLW disposal in
551 Japan, report TN1410 2000-001, Tokai-Mura.
552 Karnland, O., Nilsson, U., Weber, H., and Wersin, P., 2008. Sealing ability of Wyoming
553 bentonite pellets foreseen as buffer material-Laboratory results. Physics and Chemistry
554 of the Earth, Parts A/B/C, 33:S472–S475.
555 Kenney, T.C., van Veen, W.A., Swallow, M.A.., Sungaila, M.A., 1992. Hydraulic conductivity
556 of compacted bentonite-sand mixtures. Canadian Geotechnical Journal 29 (3):
557 364–374.
558 Komine, H., 2004. Simplified evaluation on hydraulic conductivities of sand-bentonite
559 mixture backfill. Applied Clay Science 26 (1–4), 13–19.
560 Komine, H., 2010. Predicting hydraulic conductivity of sand bentonite mixture backfill before
561 and after swelling deformation for underground disposal of radioactive wastes.
562 Engineering Geology.
563 Kröhn, K. P., 2003a. New conceptual models for the resaturation of bentonite. Applied Clay
564 Science 23 (1-4), 25-33.
565 Kröhn, K. P., 2003b. Results and interpretation of bentonite resaturation experiments with
566 liquid water and water vapour. In: Schanz, T. (Ed.), Proceedings of the International
567 Conference from Experimental Evidence towards Numerical Modeling of Unsaturated
568 Soils, Weimar, Germany, vol. 1. Springer, Berlin, pp. 257–272.
569 Krohn, K, 2004, Report GRS-199, Modelling the Re-Saturation of Bentonite in Final
570 Repositories in Crystalline Rock, ISBN 3-931995-66-6

571 Lemaire, T., Moyne, C., Stemmelen, D., 2004. Imbibition test in a clay powder (MX-80
572 bentonite. Applied Clay Science 26: 235-248.
573 Lloret, A., Villar, M.V., Sanchez, M., Gens, A.., 2003. Mechanical behaviour of heavily
574 compacted bentonite under high suction changes. Géotechnique, 53(1):27–40.
575 Loiseau, C., Cui, Y.J., Delage, P., 2002. The gradient effect on the water flow through a
576 compacted swelling soil. Proc. 3rd Int Conf Unsaturated Soils, UNSAT'2002 Recife,
577 Brazil, Balkema, vol. 1, pp. 395-400.
578 Lutz, J.F., Kemper, W.D., 1959. Intrinsic permeability of clay as afftected by clay-water
579 interaction. Soil science 88: 83-90.
580 Marcial, D., 2003. Comportement hydrome´canique et microstructural des mate´riaux de
581 barrie`re ouvrage´e. Ph.D. thesis, E ´ cole nationale des ponts et chausse´es, Paris, France
582 Miller, R.J., Low, P.F., 1963. Threshold Gradient for Water Flow in Clay Systems. Soil
583 Science Society of America Journal. 27 (6):605-609.
584 Pusch, R., 1979. Highly compacted sodium bentonite for isolating rock-deposited radioactive
585 waste products. Nucl. Technol. (United States), 45(2).
586 Pusch, R., 1999. Microstructural evolution of buffers. Engineering geology. 54:33-41.
587 Pusch, R., Yong, R., 2003. Water saturation and retention of hydrophilic clay
588 buffer-microstructural aspects.Applied Clay Science, 23:61-68.
589 Saiyouri, N., Hicher, P.Y., Tessier, D., 2000. Microstructural approach and transfer water
590 modeling in highly compacted unsaturated swelling clays. Mechanics of
591 Cohesivefrictional Materials 5, 41–60.
592 Stepkowska, E.T.: Aspects of the clay electrolyte water-system with special reference to the
593 geotechnical properties of clays. Eng. Geol. 28(3-4), 249–267 (1990)
594 Stroes-Gascoyne, S., 2010. Microbial occurrence in bentonite-based buffer, backfill and
595 sealing materials from large-scale experiments at AECL's underground research
596 laboratory. Applied Clay Science, 47(1-2):36–42.
597 Tang, A. M. & Cui, Y. J., 2005. Controlling suction by the vapour equilibrium technique at
598 different temperatures and its application in determining the water retention properties of
599 MX80 clay. Can. Geotech. J. 42 (1): 287-296.
600 Tang, C.S., Tang, A..M., Cui, Y.J., Delage, P., Barnichon, J.D., Shi, B., 2011. A study of the
601 hydro-mechanical behaviour of compacted crushed argillite. Engineering Geology. 118
602 (3-4):93-103.
603 Thomas, H.R., Cleall, P.J., Chandler, N., Dixon, D., Mitchell, H.P., 2003. Water infiltration
604 into a large-scale in-situ experiment in an underground research laboratory.
605 Geotechnique 53, 207-224.
606 Van Genuchten, M.T., 1980. A closed-form equation for predicting the hydraulic conductivity
607 of unsaturated soils. Soil Science Society of America Journal, 44: 892-898.
608 Villar, M.V.; Romero, E. & Lloret, A. 2005. Thermo-mechanical and geochemical effects on
609 the permeability of high-density clays. In: Alonso, E.E. & Ledesma, A.(eds.) Advances
610 in understanding engineered clay barriers. A.A. Balkema Publishers, Leiden: 177-191.
611 Villar, M.V., Lloret, A.., 2008. Influence of dry density and water content on the swelling of a
612 compacted bentonite. Applied Clay Science, 39(1-2):38-49.
613 Villar, M.V., Gómez-Espina, R. Campos, R., Barrios, I. & Gutiérrez-Nebot, L. 2012. Porosity
614 Changes Due To Hydration Of Compacted Bentonite. In: Mancuso, C.; Jommi, C. &

D'Onza, F. (Eds.): Unsaturated Soils: Research and Applications, Volume 1, pp. 137-144. Springer, Berlin.

Wang, Q., Tang, A. M., Cui, Y. J., Delage, P., Gatmiri. B., 2012. Experimental study on the swelling behaviour of bentonite/claystone mixture. Engineering Geology. 124:59-66.

Wang, Q., Tang, A.M., Cui, Y.J., Barnichon, J.D. Delagen P., Ye, W.M., 2013. Voids effects on the hydro-mechanical behaviour of compacted bentonite-sand mixture. *Soils and Foundations* 53(2), 232-245.

Ye, W.M., Cui, Y.J., Qian, L.X., Chen. B., 2009. An experimental study of the water transfer thro ugh confined compacted GMZ bentonite. Engineering Geology, 108(3-4):169–176.

Yong, R.N., Warkentin, B.P., 1975. Soil properties and behaviour. Elsevier, Amsterdam.

Yong, R.N., Boonsinsuk, P., and Wong, G., 1986. Formulation of backfill material for a nuclear fuel waste disposal vault. Canadian Geotechnical Journal, 23(2):216-228.

Zou, Y., 1996. A non-linear permeability relation depending on the activation energy of pore liquid. Géotechnique 46 (4), 769-774.

List of Tables

Table 1. Chemical composition of the synthetic water
Table 2. Tests performed for water retention property and microstructure observation

List of Figures

Figure 1. Grain size distribution of the MX80 bentonite and sand
Figure 2. Schematic setup of the infiltration cell
Figure 3. Constant volume cell for WRC determination; (a) osmotic method; (b) vapour equilibrium technique
Figure 4. WRCs of bentonite/sand mixture under constant-volume conditions
Figure 5 Water content and dry density distributions after dismantling of the sample
Figure 6. Evolution of relative humidity during water infiltration
Figure 7. Suction profiles at different times
Figure 8. Determination of hydraulic gradient and water flux: (a) hydraulic gradient; (b) rate of water flow
Figure 9. Calculated and measured water volume into the sample
Figure 10. Hydraulic conductivity versus suction for different measurement sections
Figure 11. Pore size distributions of the bentonite-sand mixture wetted with different suctions under constant volume conditions
Figure 12. SEM photographs of bentonite/sand mixture samples equilibrated at different suctions
Figure 13. Water flux versus hydraulic gradient for different suctions
Figure 14. Hydraulic conductivity versus suction
Figure 15. Changes of large-pore void ratio with suction

667 Table 1. Chemical composition of the synthetic water

Components	$NaHCO_3$	Na_2SO_4	NaCl	KCl	$CaCl_2.2H_2O$	$MgCl_2.6H_2O$	$SrCl_2.6H_2O$
Mass (g) per litre of solution	0.28	2.216	0.615	0.075	1.082	1.356	0.053

668

669 Table 2. Tests performed for water retention property and microstructure observation

Suction (MPa)	Suction control method and duration	Microstructure	
		MIP	SEM
38	Vapour (2 months)	√	√
24.9		√	
12.6		√	
9.0			
4.2		√	√
1	Osmotic (2 months)	√	
0.1			
0	Distilled water (2 months)	√	√
65	Initial suction	√	√

670

671

672

673

674

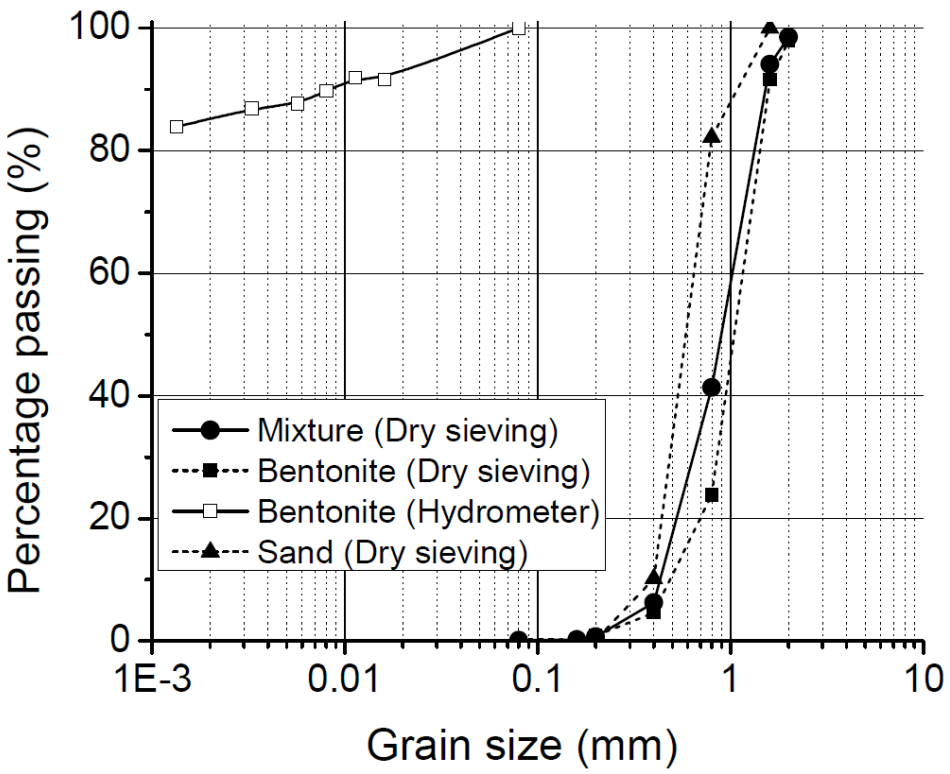

675

676 Figure 1. Grain size distribution of the MX80 bentonite and sand

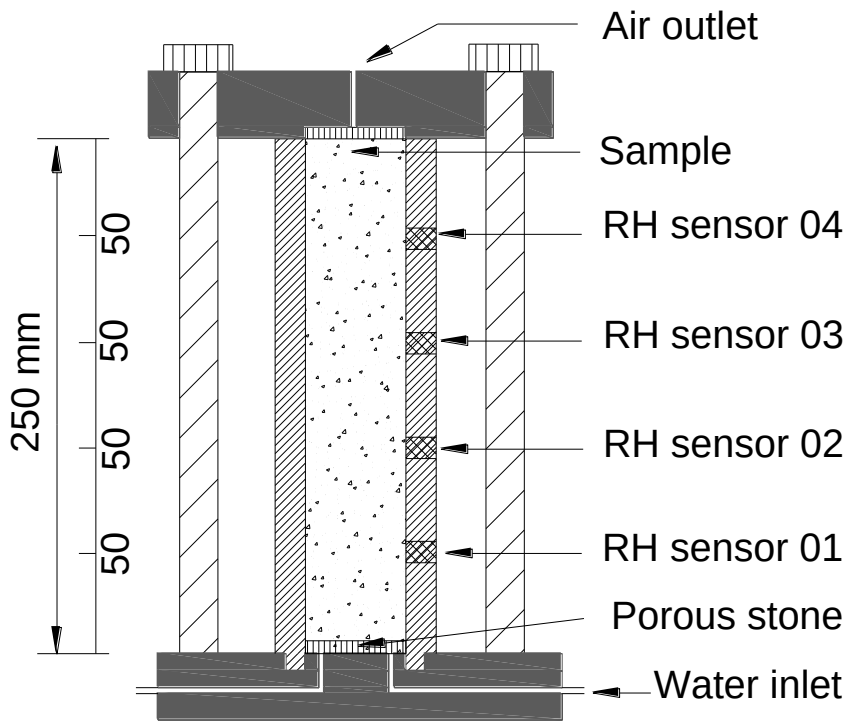

677

678 Figure 2. Schematic setup of the infiltration cell

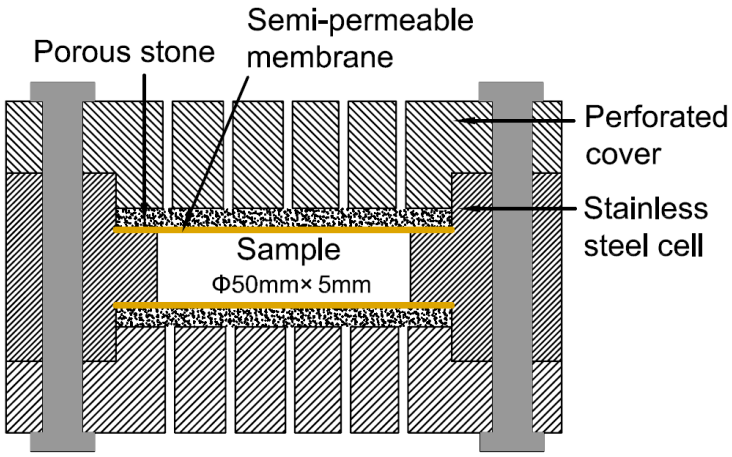

(a)

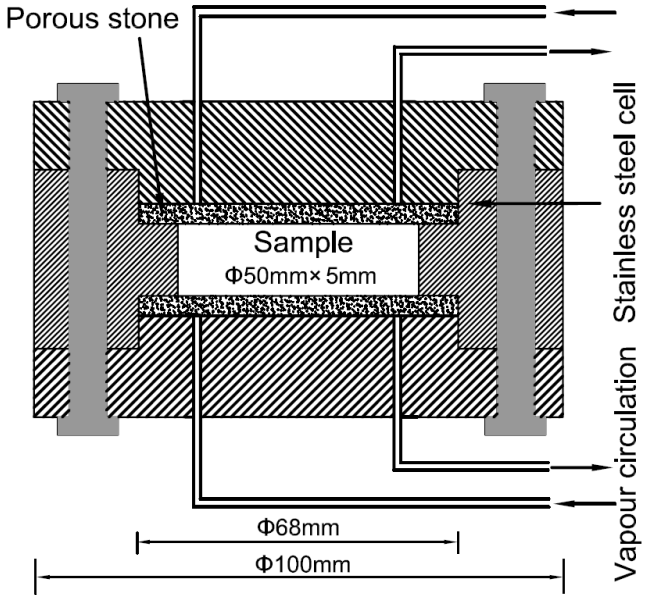

(b)

Figure 3. Constant volume cell for WRC determination; (a) osmotic method (controlling of matric suction); (b) vapour equilibrium technique (controlling of total suction)

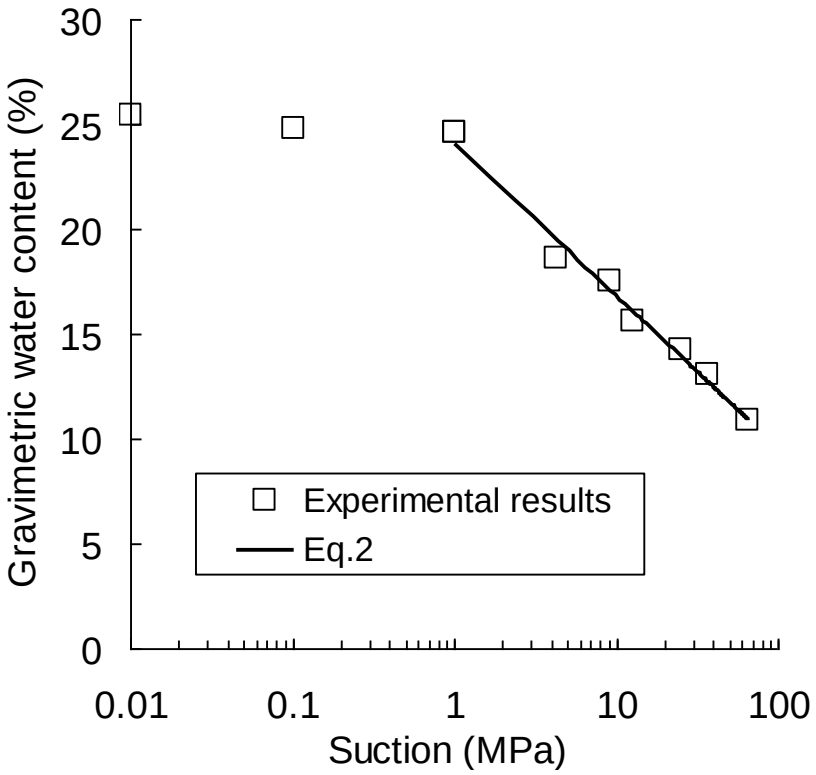

685

686 Figure 4. WRC of bentonite/sand mixture under constant-volume conditions

687

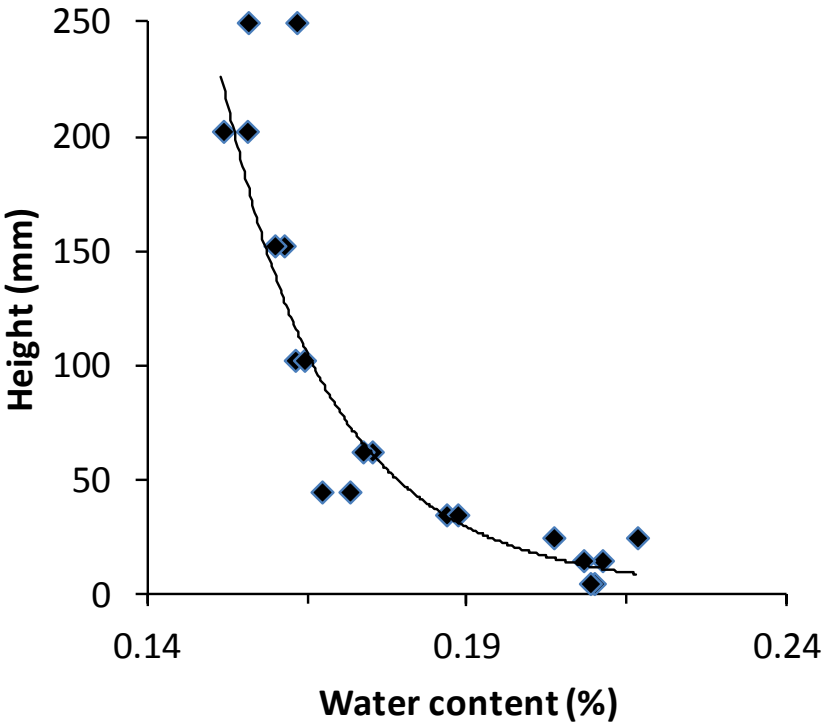

688

689 (a) water content distribution

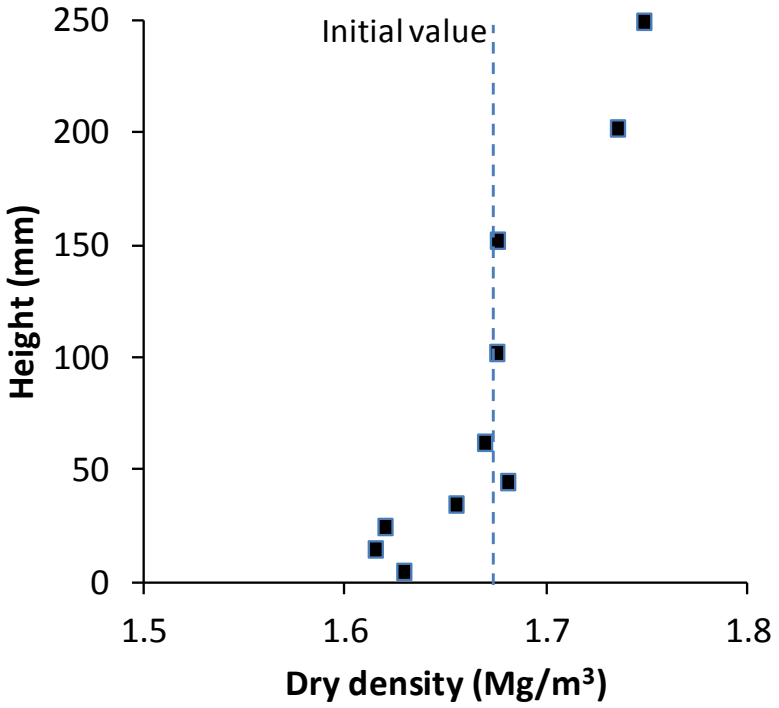

690

691 (b) dry density distribution

692 Figure 5 Water content and dry density distributions after dismantling of the sample

693

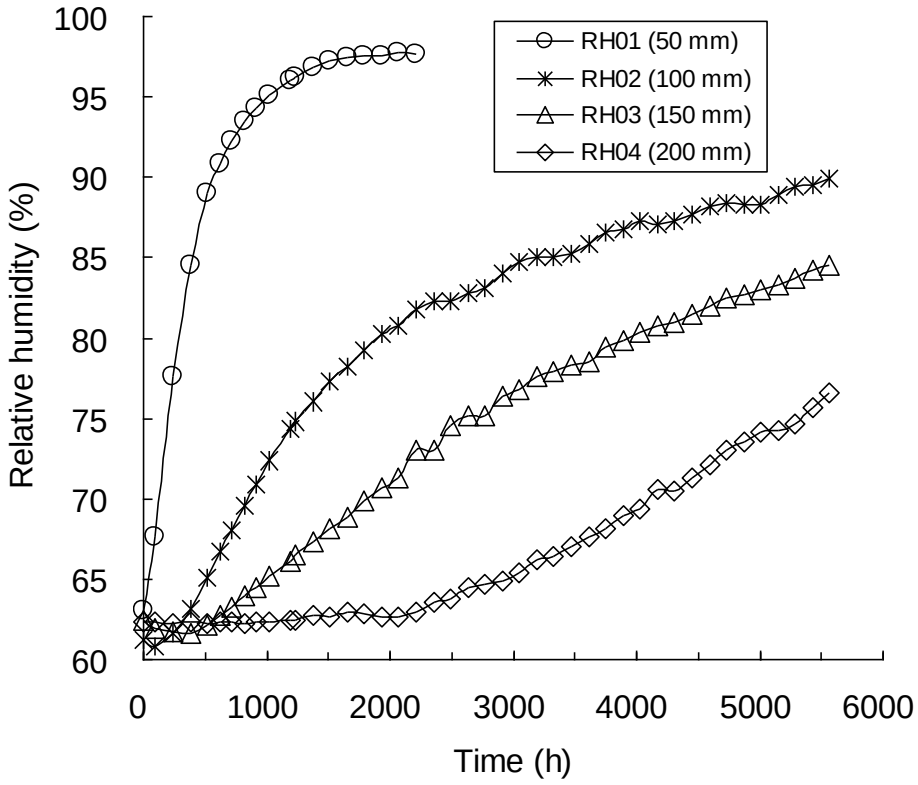

694

695 Figure 6. Evolution of relative humidity during water infiltration

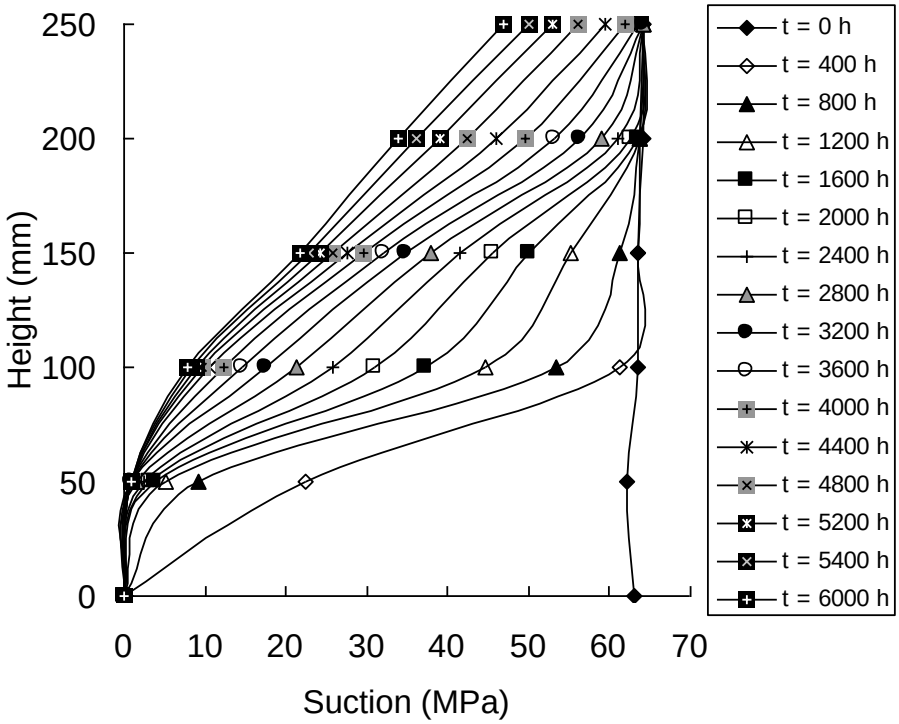

696

697 Figure 7. Suction profiles at different times (Note: There were no measurements at height 250 mm.
698 The values plotted in the figure were extrapolated from the measurements at lower heights)

699

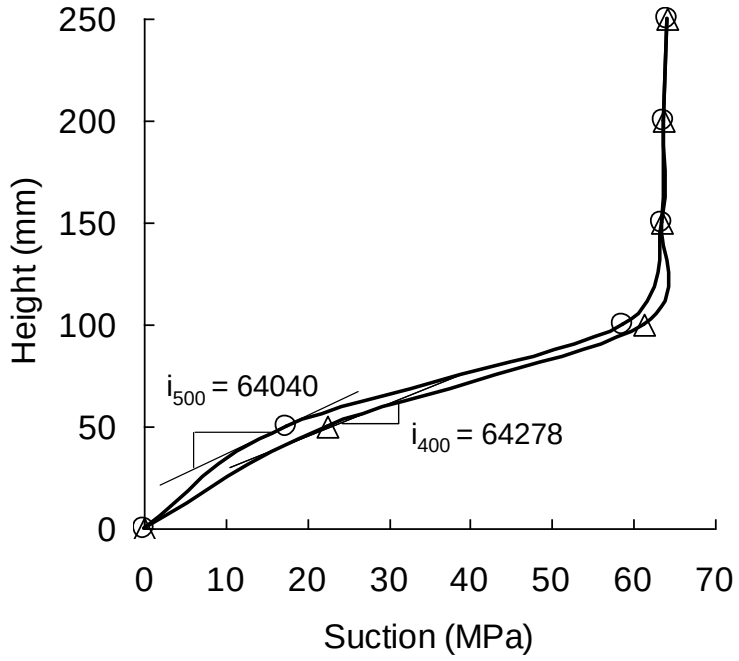

700

701 (a)

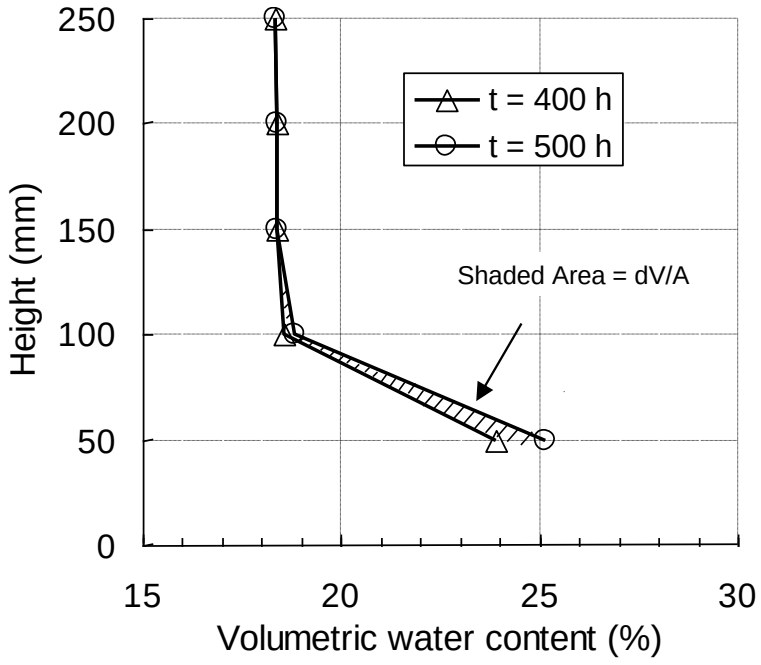

702

703 (b)

704 Figure 8. Determination of hydraulic gradient and water flux for two times (400 and 500 h)
705 during infiltration: (a) hydraulic gradient; (b) rate of water flow

706

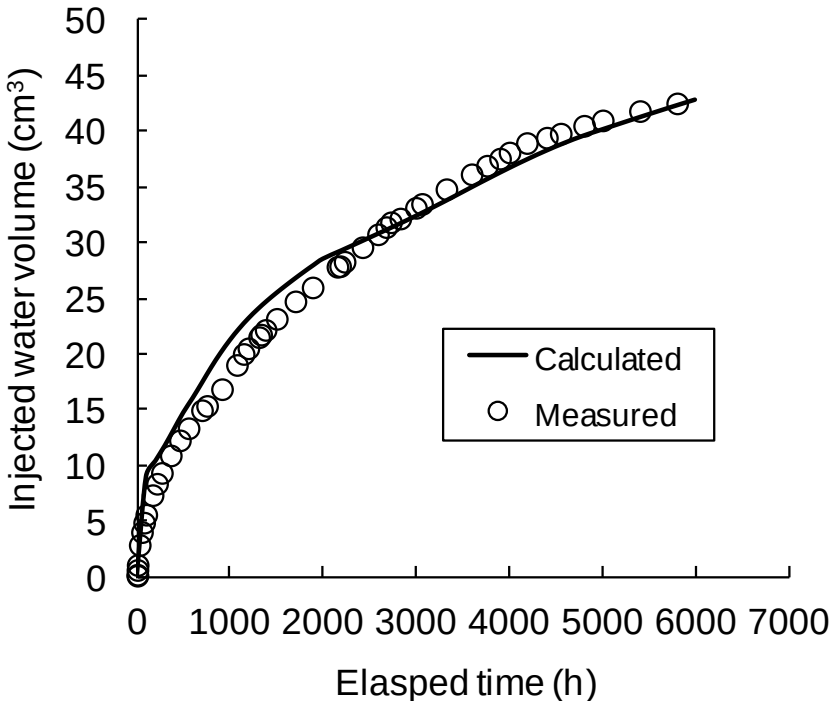

707

708 Figure 9. Calculated and measured water volume into the sample

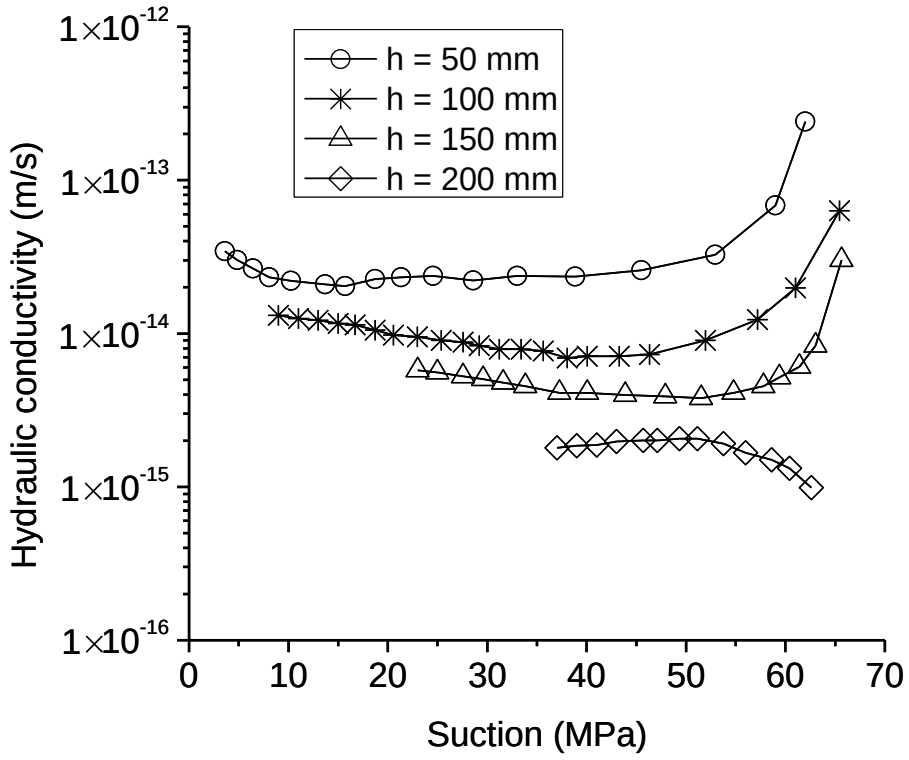

709

710 Figure 10. Hydraulic conductivity versus suction for different measurement sections ("h"
711 represents the distance from hydration surface

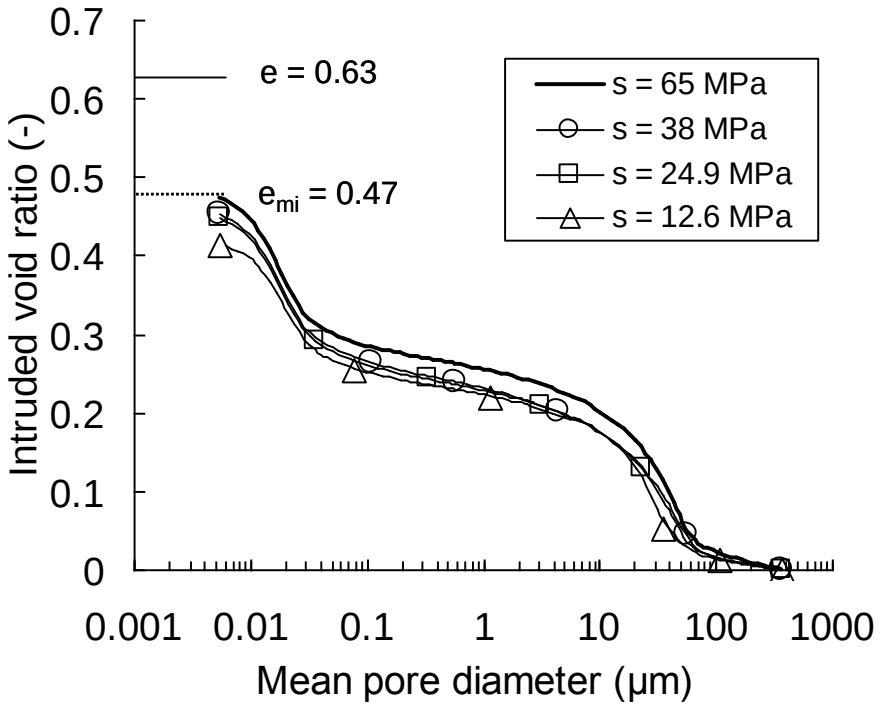

712

713 (a) 65 - 12.6 MPa suction

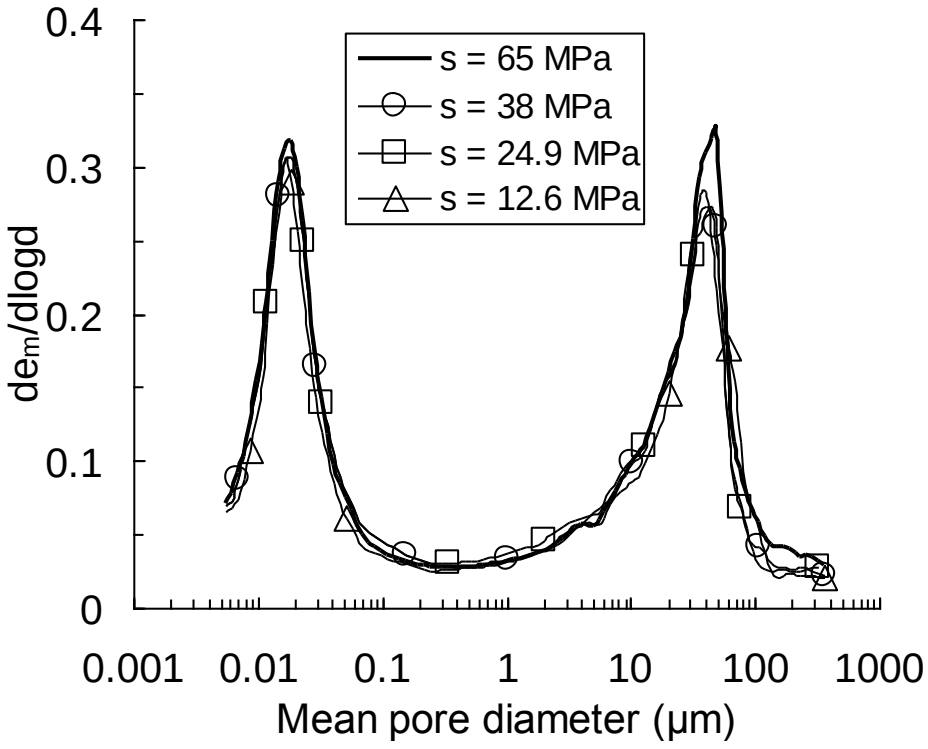

714

715 (b) 65 - 12.6 MPa suction

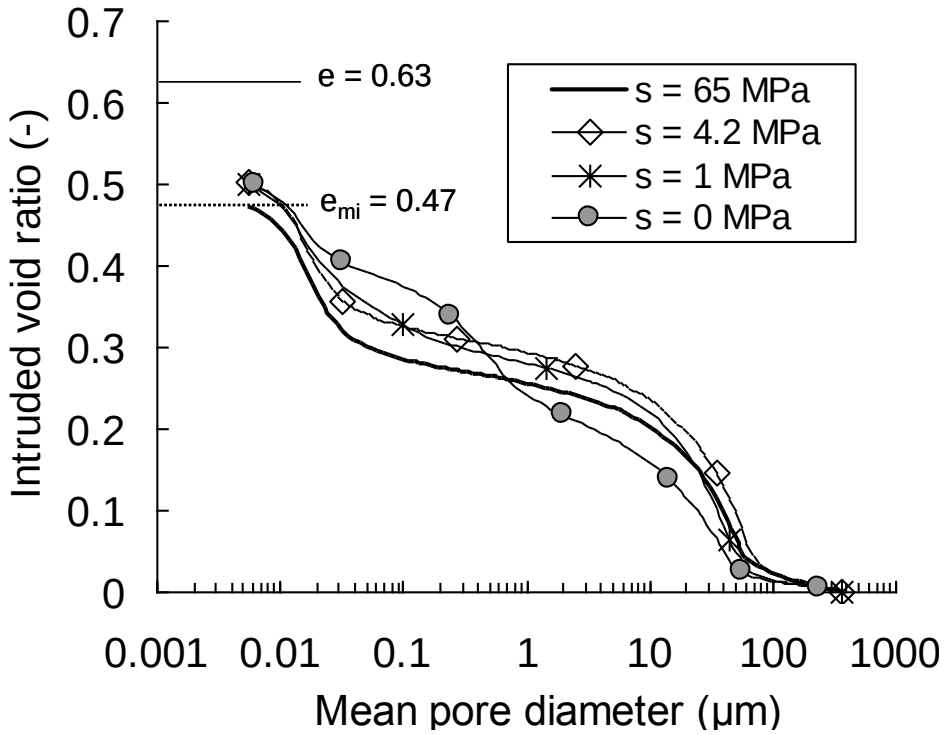

716

717 (c) 4.2 – 0 MPa suction

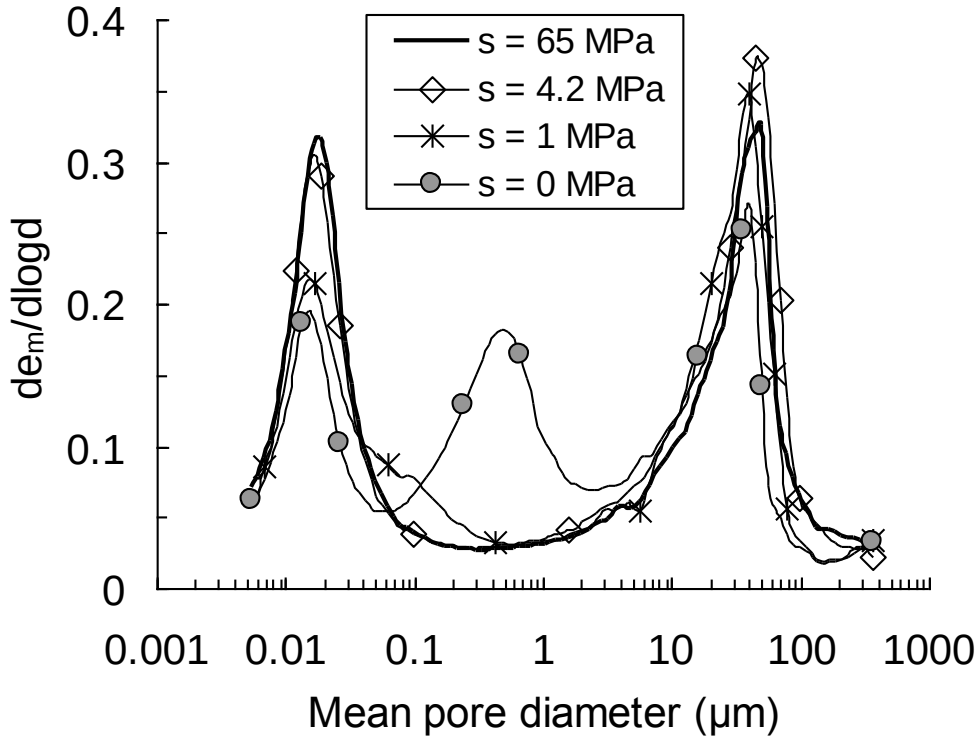

718

719 (d) 4.2 – 0 MPa suction

720 Note: symbols plotted in the figure do not correspond to all the measurement points, just a few
721 symbols in each curve are plotted for distinction.

722 Figure 11. Pore size distributions of the bentonite-sand mixture wetted with different suctions

723 under constant volume conditions

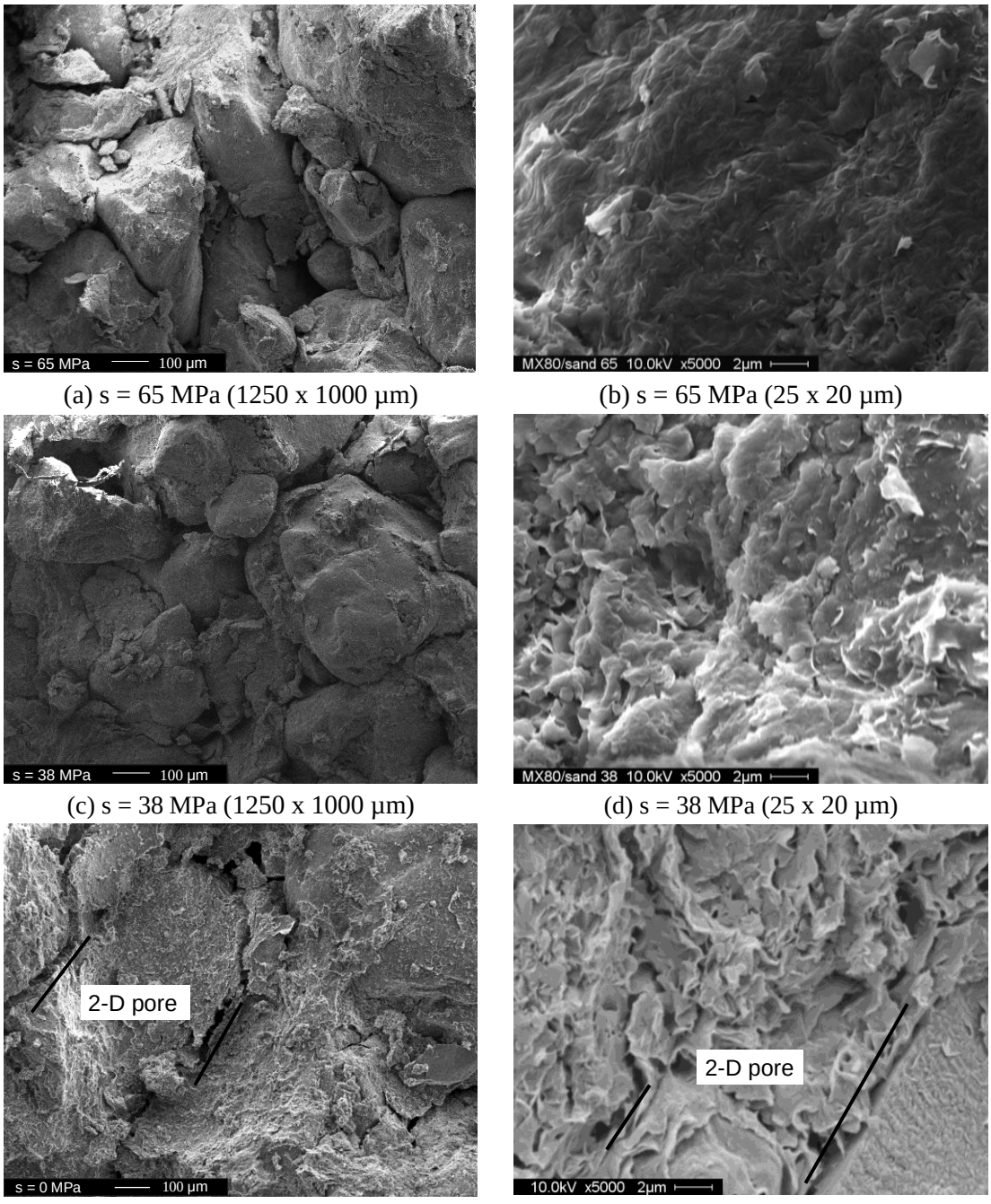

(a) s = 65 MPa (1250 x 1000 µm) (b) s = 65 MPa (25 x 20 µm)

(c) s = 38 MPa (1250 x 1000 µm) (d) s = 38 MPa (25 x 20 µm)

(e) s = 0 MPa (1250 x 1000 µm) (f) s = 0 MPa (25 x 20 µm)

724 Figure 12. SEM photographs of bentonite/sand mixture samples equilibrated at different
725 suctions

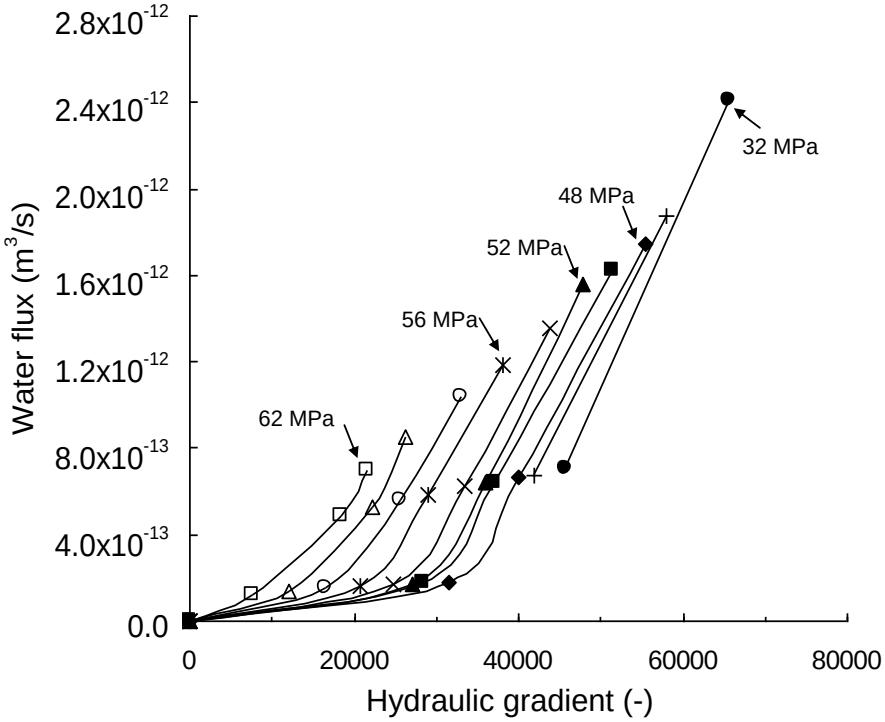

726

727 Figure 13. Water flux versus hydraulic gradient for different suctions

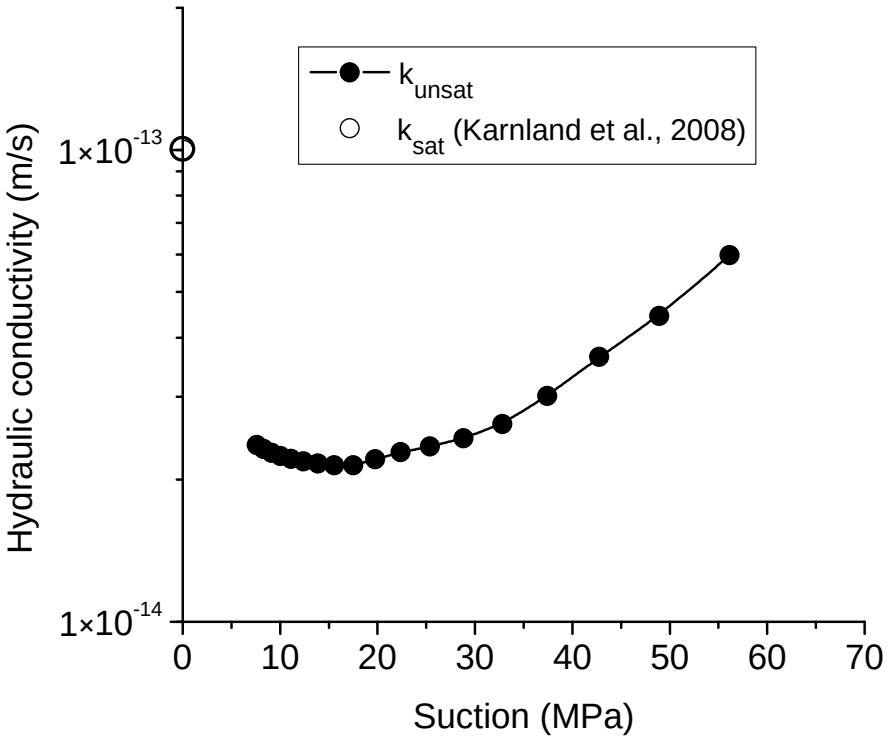

728

729 Figure 14. Hydraulic conductivity versus suction

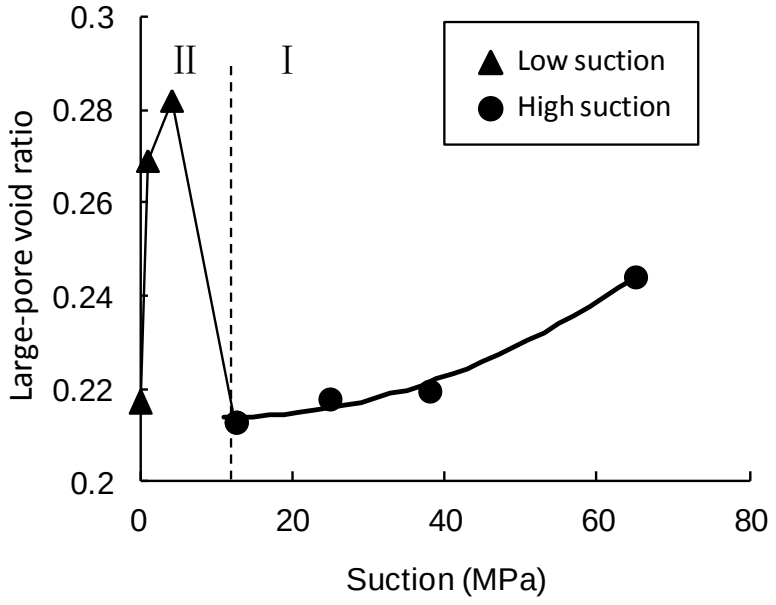

730

731 Figure 15. Changes of large-pores void ratio (diameter larger than 2 μm) with suction